

Measurements of charged-particle multiplicity dependence of higher-order net-proton cumulants in $p+p$ collisions at $\sqrt{s} = 200$ GeV from STAR at RHIC

The STAR Collaboration

We report on the charged-particle multiplicity dependence of net-proton cumulant ratios up to sixth order from $\sqrt{s} = 200$ GeV $p+p$ collisions at the Relativistic Heavy Ion Collider (RHIC). The measured ratios C_4/C_2 , C_5/C_1 , and C_6/C_2 decrease with increased charged-particle multiplicity and rapidity acceptance. Neither the Skellam baselines nor PYTHIA8 calculations account for the observed multiplicity dependence. In addition, the ratios C_5/C_1 and C_6/C_2 approach negative values in the highest-multiplicity events. The negative ratios in the most central $p+p$ collisions at 200 GeV, similar to those observed in central Au+Au 200 GeV collisions, imply the formation of thermalized QCD matter.

Exploring the quantum chromo-dynamics (QCD) phase structure is one of the ultimate goals in heavy-ion collision experiments. The QCD phase diagram is characterized in terms of temperature (T) for the x-axis and baryon chemical potential (μ_B) for the y-axis. In the conjectured structure of the QCD phase diagram, there is a quark-gluon plasma (QGP) phase from the upper left to the upper right quadrant where the thermalized QCD matter is formed, while a hadron gas phase exists at the lower left quadrant. However, the transition between the two phases is not well-understood. According to lattice-QCD calculations, the phase transition at $\mu_B/T < 2$ is likely a smooth crossover [1, 2]. However, model calculations predict a first-order phase transition in the finite μ_B region [3] as well as a QCD critical point [4].

Cumulants of conserved charges are believed to be sensitive to the QCD phase structure [5]. Various orders cumulants (C_n , $n \leq 6$), of net-proton, net-kaon, and net-charge multiplicity distributions have been measured by the ALICE, STAR, HADES, and NA61/SHINE collaborations [6–13]. The net-proton C_4/C_2 in the Beam Energy Scan program phase I (BES-I) ($7.7 < \sqrt{s_{NN}} < 200$ GeV) at RHIC indicates a non-monotonic collision-energy dependence with 3.1σ significance, which hints at the existence of a critical point at $\sqrt{s_{NN}} < 20$ GeV [14]. The ratios including C_2/C_1 , C_3/C_2 , and C_4/C_2 reported from the STAR and HADES collaborations at 2.4 and 3.0 GeV Au+Au collisions are consistent with those from hadronic interactions and baryon-number conservation according to the Ultrarelativistic Quantum Molecular Dynamics (UrQMD) model [15, 16]. Data have been taken during the STAR Beam Energy Scan program phase II (BES-II) with fixed-target runs to fill the gap for $3.0 < \sqrt{s_{NN}} < 7.7$ GeV, albeit with significant differences in acceptance compared to the collider mode data-taking.

Higher-order cumulant ratios have been measured by STAR for Au+Au collisions at $\sqrt{s_{NN}} = 200$ GeV. In particular, the ratios C_6/C_2 were found to be systematically negative from peripheral to central collisions. The negative values are qualitatively consistent with QCD models and lattice QCD calculations [17–19] which suggest a smooth crossover transition.

This Letter reports the net-proton cumulant ratios, C_2/C_1 , C_3/C_2 , C_4/C_2 , C_5/C_1 , and C_6/C_2 measured in $p+p$ collisions at $\sqrt{s} = 200$ GeV, which provides baselines for comparison with Au+Au collisions. Experimental results from RHIC and the Large Hadron Collider (LHC) suggest that strongly-interacting matter may be formed

in high-multiplicity $p+p$ collisions [20, 21]. This scenario can be tested by measuring the multiplicity dependence of higher-order cumulant ratios. It should be also noted that, even if collectivity of multiple particles exists in $p+p$ collisions, it does not necessarily indicate that the thermalized QCD drops of matter have been created. This can be tested by comparing various order of cumulants between data and thermal model calculations [22].

The data set was taken in 2012 using a minimum-bias trigger, with 220 million events analyzed. All data were measured using the Time Projection Chamber (TPC) and Time of Flight (TOF) detector at the STAR experiment [23]. The collision vertex is required to be within 30 cm of the detector center and within 2 cm in the transverse direction relative to the beamline. Pileup events are suppressed by requiring the difference in the vertex position along the beamline measured by the TPC and the Vertex Position Detector to be within ± 3 cm, and by requiring that tracks are matched to the TOF hits. Protons and antiprotons are analyzed in the transverse momentum range $0.4 < p_T < 2.0$ GeV/ c and in the midrapidity acceptance $|y| < 0.5$. Figure 1 (a) shows the ionization energy loss (dE/dx) as a function of the momentum of charged particles, as measured by the TPC. Figure 1 (b) depicts correlations between mass squared (m^2) measured by the TOF and the momentum measured by the TPC. Protons and antiprotons are identified by using both dE/dx and m^2 . The distance of closest approach of a reconstructed track to the collision vertex is required to be less than 1 cm to suppress the contribution from secondary protons from weak decays. Cumulants are calculated at each bin of measured charged-particle multiplicity, m_{ch}^{TT} , which is defined as charged tracks having hits both in the TPC and TOF at midrapidity. Protons and antiprotons are excluded from m_{ch}^{TT} in order to suppress self-correlations [24]. The m_{ch}^{TT} distribution is shown in Fig. 1 (c). The event-by-event net-proton number distributions for two ranges of m_{ch}^{TT} are shown in Fig. 1 (d). The TOF hit requirement is designed to suppress the contribution from collision pileup events in high-luminosity $p+p$ collisions. Since the efficiency of the TOF is well understood in the experiment [9], m_{ch}^{TT} is converted to the corresponding multiplicity in the TPC, m_{ch}^{TPC} , in subsequent discussions, as the new results will be finally compared with previous measurements from Au+Au collisions [25].

The n th-order cumulant is defined by the n th derivatives of the cumulant-generating function. Explicitly, cu-

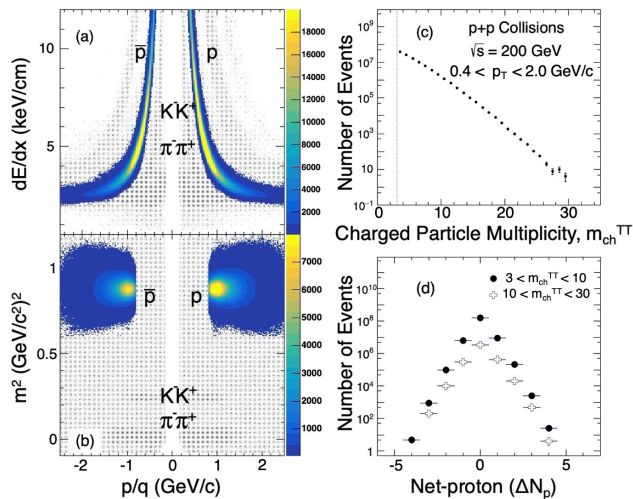


FIG. 1. (a) Correlations between the energy loss, dE/dx , of charged tracks measured by the TPC and momentum divided by electric charge. (b) Correlations between the mass squared, m^2 , measured by the TOF and the ratio of momentum to the electric charge, p/q . Contour bands represent the identified protons and antiprotons used in the analysis, while black solid circles are for other charged particles. (c) Charged-particle multiplicity distribution. (d) Event-by-event net-proton multiplicity distributions for $|y| < 0.5$ and $0.4 < p_T < 2.0$ GeV/c at two ranges of charged particle multiplicity as indicated in the legend.

mulants are expressed in Eqs. (1)-(6).

$$C_1 = \langle N \rangle, \quad (1)$$

$$C_2 = \langle (\delta N)^2 \rangle, \quad (2)$$

$$C_3 = \langle (\delta N)^3 \rangle, \quad (3)$$

$$C_4 = \langle (\delta N)^4 - 3\langle (\delta N)^2 \rangle^2 \rangle, \quad (4)$$

$$C_5 = \langle (\delta N)^5 - 10\langle (\delta N)^3 \rangle \langle (\delta N)^2 \rangle \rangle, \quad (5)$$

$$C_6 = \langle (\delta N)^6 - 15\langle (\delta N)^4 \rangle \langle (\delta N)^2 \rangle - 10\langle (\delta N)^3 \rangle^2 + 30\langle (\delta N)^2 \rangle^3 \rangle, \quad (6)$$

where $\langle \delta N \rangle = N - \langle N \rangle$, N is the number of particles in one event, and the angle brackets indicate the average over all events.

The cumulant ratios, C_2/C_1 , C_3/C_2 , C_4/C_2 , C_5/C_1 , and C_6/C_2 , are employed to cancel the trivial volume dependence of cumulants [26]. Neutrons cannot be measured in the STAR experiment, hence net-proton number is measured as a proxy for net-baryon number [27]. A Skellam distribution, which is defined as the difference between two independent Poisson distributions, is employed as a statistical baseline. The odd- and even-order cumulants of the Skellam distribution are expressed by the difference and the sum of the averaged values of protons and antiprotons, respectively. Consequently, the Skellam baselines for C_4/C_2 , C_5/C_1 , and C_6/C_2 are always unity, while the corresponding baselines for C_2/C_1 and C_3/C_2 depend on the averaged value of protons and antiprotons.

In order to account for detector efficiency effects present in cumulants calculated from Fig. 1 (d), efficiency corrections are applied to the measured cumulants including luminosity, acceptance, and charged-particle

multiplicity dependencies [28]. The detector efficiencies are assumed to follow binomial distributions [27, 29–35]. Statistical uncertainties are estimated by the bootstrap method [33, 36]. Systematic uncertainties are estimated by varying the selection ranges for track quality, particle identification, luminosity, and by varying the detector efficiencies for the efficiency corrections. The luminosity ranges from 2 kHz to 15 kHz for the coincidence rates for the Zero Degree Calorimeters, which is divided into 10 groups to estimate the variations of the cumulants. A Barlow test was performed in order to remove contribution from statistical uncertainties [37]. The systematic uncertainties from each source are 0.29, 0.32, 0.38, and 0.69 %, respectively, for multiplicity-averaged results of C_4/C_2 . The total systematic uncertainties are 0.90, 7.8, and 8.4% for C_4/C_2 , C_5/C_1 , and C_6/C_2 , respectively.

Charged-particle multiplicity dependence for the net-proton cumulant ratios, C_4/C_2 , C_5/C_1 , and C_6/C_2 are shown in Fig. 2 as red dots. Vertical bars represent statistical uncertainties while the red bands represent systematic uncertainties. The main source of the large systematic uncertainties for each charged-particle multiplicity bin is the luminosity. It constitutes 50% out of total systematic uncertainty for C_4/C_2 at $m_{ch}^{TPC} = 4$, which increases up to above 90% at $m_{ch}^{TPC} > 18$. The effect is more prominent for C_5/C_1 and C_6/C_2 , greater than 90% in most m_{ch}^{TPC} bins. Calculations from the Skellam baseline and PYTHIA8 model [38] are shown as black dashed lines and purple bands, respectively. Approximately 800 million PYTHIA8 events, with the option of SoftQCD, are generated for the comparison. Figure 2 indicates all ratios are decreasing with increasing multiplicity, except for C_2/C_1 . Although the PYTHIA8 model shows multiplicity dependence, it fails to reproduce the observed multiplicity dependence, especially at high multiplicities. For the higher-order ratios C_4/C_2 , C_5/C_1 , and C_6/C_2 , the model (purple squares) also overpredicts the multiplicity-averaged data values (cyan solid circles).

As reported in Ref. [39], thermodynamic model calculations from both lattice QCD [1, 19] and functional renormalization group (FRG) [18] predict a special ordering of the higher-order baryon-number susceptibility ratios: $\chi_4^B/\chi_2^B > \chi_5^B/\chi_1^B > \chi_6^B/\chi_2^B$. The multiplicity-averaged ratios in Fig. 2 show the hierarchy $C_4/C_2 > C_5/C_1 > C_6/C_2$, where the significance of the first and second inequalities is 8.7σ and 0.9σ , respectively. At high charged-particle multiplicity bins $m_{ch}^{TPC} > 12$, both values of C_5/C_1 and C_6/C_2 are consistent with zero within uncertainties, which hints at a possible sign change in these ratios. These observations are consistent with the thermodynamic model expectation for the formation of thermalized QCD matter in high-multiplicity $p+p$ collisions. We discuss this point later when comparing with results from 200 GeV Au+Au collisions.

Note that the PYTHIA8 calculations fail to reproduce the hierarchy in the ratios and no hint of a sign change is observed. At LHC energies, due to multi-parton interactions in $p+p$ collisions, the color-reconnection (CR) mechanism is used to mimic collective excitation for strangeness and heavy-quark production [40–45]. In this case, PYTHIA8 calculations with CR included do not have any significant effect on the net-proton higher-order cumulant ratios from the 200 GeV $p+p$ collisions.

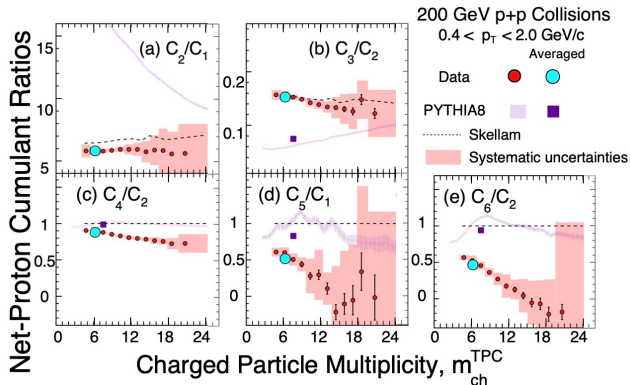


FIG. 2. Net-proton cumulant ratios, C_2/C_1 , C_3/C_2 , C_4/C_2 , C_5/C_1 , and C_6/C_2 as a function of charged-particle multiplicity from $\sqrt{s} = 200$ GeV $p+p$ collisions. Cyan points represent event averages for $3 \leq m_{\text{ch}} < 30$, and they are plotted at the corresponding value of $m_{\text{ch}}^{\text{TPC}}$. The uncertainties on the cyan points are smaller than the marker size. The Skellam baselines are shown as dashed lines. The results of the PYTHIA8 calculations are shown as purple bands. Purple squares are event-averaged values from the model calculations.

Studying the rapidity dependence of the cumulant ratios may shed light on the time evolution of the collision dynamics [46]. The rapidity-window dependence of the net-proton cumulant ratios vs. multiplicity is shown in Fig. 3, with the colored solid circles representing data from three rapidity bins. In order to avoid overlapping uncertainties, data are plotted up to $m_{\text{ch}}^{\text{TPC}} = 14$. Multiplicity-averaged values from the smallest and largest rapidity bins are shown as cyan squares and circles, respectively. The higher-order ratios C_4/C_2 , C_5/C_1 , and C_6/C_2 show that the larger the rapidity acceptance, the more the ratios deviate from the corresponding ratio of the Skellam distribution (dashed lines) and the values are largely decreasing with increasing multiplicity. Both features imply the strongest correlation in the largest rapidity window. A similar rapidity-window dependence has also been observed in Au+Au collisions at RHIC [47]. In addition, in the widest rapidity bin, $|y| < 0.5$, the ratios C_5/C_1 and C_6/C_2 approach negative values at the highest multiplicity, indicating that thermalized QCD matter may be created in very high-multiplicity events in $p+p$ collisions at RHIC. None of the observations are reproduced by the QCD-inspired event generator PYTHIA8, which implies a lack of collective excitation dynamics in the model.

Net-proton ratios C_4/C_2 , C_5/C_1 , and C_6/C_2 are compared with those from Au+Au collisions at $\sqrt{s_{\text{NN}}} = 200$ GeV [47] in Fig. 4, shown as a function of the charged-particle multiplicity. The kinematic acceptance $0.4 < p_{\text{T}} < 2.0$ GeV/ c and $|y| < 0.5$ is used in both $p+p$ and Au+Au collisions. The five data points for Au+Au collisions correspond to 0-40%, 40-50%, 50-60%, 60-70%, and 70-80% centrality bins. The ratios from $p+p$ collisions have a steeper dependence on the multiplicity than those from Au+Au collisions. The ratios from averaging the $p+p$ collisions seem to follow the trend from the peripheral Au+Au collisions. The ratios from $p+p$ collisions decrease with increasing multiplicity. In particular, both the ratios C_5/C_1 and C_6/C_2 from $p+p$ collisions decrease with multiplicity, approach negative values for

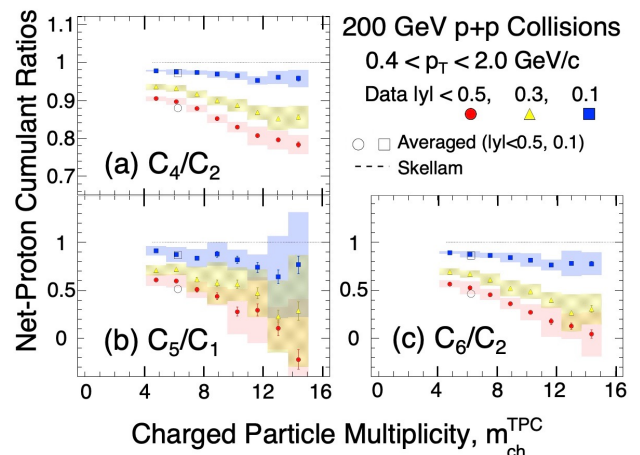


FIG. 3. Rapidity-acceptance dependence of the net-proton cumulant ratios shown as a function of the charged-particle multiplicity, $m_{\text{ch}}^{\text{TPC}}$, from $\sqrt{s} = 200$ GeV $p+p$ collisions. For $|y| < 0.5$, the mean multiplicity is found to be $\langle m_{\text{ch}}^{\text{TPC}} \rangle = 6.23$. The multiplicity-averaged values from $|y| < 0.1$ and $|y| < 0.5$ are shown as cyan squares and circles, respectively. The Skellam baselines are shown as dashed lines.

the highest-multiplicity events. The negative ratios in the context of lattice QCD calculations imply that even in the small $p+p$ system, thermalized QCD matter may be created in the highest-multiplicity collisions. Similar phenomena have been observed in the multiplicity dependence of strange hadron and J/ψ production [41–43], as well as the long-range collective motion [44, 45] in $p+p$ collisions at LHC energies. Overall, the high-order net-proton cumulant ratios from both 200 GeV $p+p$ and Au+Au collisions show a clear decreasing trend from low to high charged-particle multiplicity, and eventually reach values consistent with lattice QCD calculations assuming $\mu_{\text{B}} = 25$ MeV and $T = 155$ MeV [48], within uncertainties. While it may be possible to create thermalized QCD matter in high-multiplicity $p+p$ collisions at RHIC, the detailed dynamics to reach thermalization could be different from those for peripheral and central Au+Au collisions. Measurements of the cumulant ratios at high center-of-mass energies or in larger collision system than $p+p$, (e.g. $p+\text{Au}$, $d+\text{Au}$, $\text{Zr}+\text{Zr}$, and $\text{Ru}+\text{Ru}$ collision systems) could provide systematic information on the dynamics of the observed multiplicity dependence.

In summary, we report the first measurements of higher-order cumulant ratios C_2/C_1 , C_3/C_2 , C_4/C_2 , C_5/C_1 and C_6/C_2 of net-proton multiplicity distributions in $p+p$ collisions at $\sqrt{s} = 200$ GeV, as measured by the STAR detector at RHIC. Both charged-particle multiplicity and rapidity-cut dependencies are reported. It is found that the ratios are all below Skellam expectations. Calculations from PYTHIA8 [38] fail to reproduce the multiplicity dependence and the hierarchy observed in net-proton ratios C_4/C_2 , C_5/C_1 and C_6/C_2 . Within uncertainties, the multiplicity dependence of these ratios is found to be smoothly connected to the results from Au+Au collisions at $\sqrt{s_{\text{NN}}} = 200$ GeV. Overall, the net-proton cumulant ratios C_4/C_2 , C_5/C_1 and C_6/C_2 decrease progressively between the 200 GeV $p+p$ collisions and Au+Au central collisions. In the currently-measured highest-multiplicity bin, the ratios

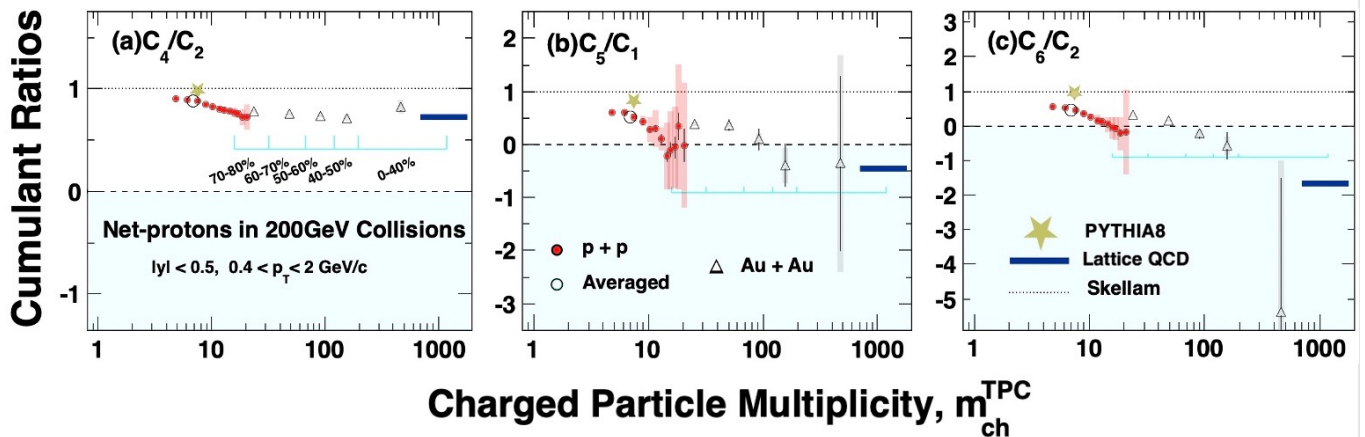


FIG. 4. Net-proton cumulant ratios, C_4/C_2 , C_5/C_1 , and C_6/C_2 as a function of charged-particle multiplicity for $p+p$ collisions and Au+Au collisions at 200 GeV for $|y| < 0.5$ and $0.4 < p_T < 2.0$ GeV/ c . Cyan circles represent event averages for $3 \leq m_{ch}^{TPC} < 30$ from the $p+p$ collisions. Results from Au+Au collisions are shown as triangles for the 0-40%, 40-50%, 50-60%, 60-70%, and 70-80% centrality bins. Red and orange bands show the systematic uncertainties for $p+p$ collisions and Au+Au collisions, respectively. The Skellam baselines are shown in long-dashed lines. The navy bands show corresponding susceptibility ratios of baryon number from lattice QCD calculations [19], where the multiplicity range is chosen arbitrarily.

C_5/C_1 and C_6/C_2 from $p+p$ collisions are consistent with zero within large uncertainties, approaching negative values at higher-multiplicity region. While the multiplicity-averaged ratios from $p+p$ collisions remain positive, the results of Au+Au central collisions are negative and qualitatively consistent with lattice QCD calculations. Systematic measurements of the cumulant ratios from higher collision energies, in larger colliding systems, and wider acceptance in rapidity will provide important information on the underlying dynamics of high-order net-proton cumulants and the process of thermalization in high-energy collisions.

We thank the RHIC Operations Group and RCF at BNL, the NERSC Center at LBNL, and the Open Science Grid consortium for providing resources and support. This work was supported in part by the Office of Nuclear Physics within the U.S. DOE Office of Science, the U.S.

National Science Foundation, National Natural Science Foundation of China, Chinese Academy of Science, the Ministry of Science and Technology of China and the Chinese Ministry of Education, the Higher Education Sprout Project by Ministry of Education at NCKU, the National Research Foundation of Korea, Czech Science Foundation and Ministry of Education, Youth and Sports of the Czech Republic, Hungarian National Research, Development and Innovation Office, New National Excellence Programme of the Hungarian Ministry of Human Capacities, Department of Atomic Energy and Department of Science and Technology of the Government of India, the National Science Centre and WUTID-UB of Poland, the Ministry of Science, Education and Sports of the Republic of Croatia, German Bundesministerium für Bildung, Wissenschaft, Forschung und Technologie (BMBF), Helmholtz Association, Ministry of Education, Culture, Sports, Science, and Technology (MEXT) and Japan Society for the Promotion of Science (JSPS).

-
- [1] S. Borsanyi, Z. Fodor, J. N. Guenther, S. K. Katz, K. K. Szabo, A. Pasztor, I. Portillo, and C. Ratti, *JHEP* **10**, 205 (2018), arXiv:1805.04445 [hep-lat].
- [2] Y. Aoki, G. Endrodi, Z. Fodor, S. D. Katz, and K. K. Szabo, *Nature* **443**, 675 (2006), arXiv:hep-lat/0611014 [hep-lat].
- [3] E. S. Bowman and J. I. Kapusta, *Phys. Rev.* **C79**, 015202 (2009), arXiv:0810.0042 [nucl-th].
- [4] M. A. Stephanov, *Phys. Rev. Lett.* **107**, 052301 (2011).
- [5] M. A. Stephanov, *Phys. Rev. Lett.* **102**, 032301 (2009), arXiv:0809.3450 [hep-ph].
- [6] L. Adamczyk *et al.* (STAR), *Phys. Rev. Lett.* **112**, 032302 (2014), arXiv:1309.5681 [nucl-ex].
- [7] L. Adamczyk *et al.* (STAR), *Phys. Rev. Lett.* **113**, 092301 (2014), arXiv:1402.1558 [nucl-ex].
- [8] L. Adamczyk *et al.* (STAR), (2017), arXiv:1709.00773 [nucl-ex].
- [9] M. Abdallah *et al.* (STAR), *Phys. Rev. C* **104**, 024902 (2021), arXiv:2101.12413 [nucl-ex].
- [10] J. Adam *et al.* (STAR), *Phys. Rev. Lett.* **126**, 092301 (2021), arXiv:2001.02852 [nucl-ex].
- [11] M. Maćkowiak-Pawłowska (NA61/SHINE), in *International Conference on Critical Point and Onset of Deconfinement* (2021) arXiv:2111.05042 [nucl-ex].
- [12] J. Adamczewski-Musch *et al.* (HADES), *Phys. Rev. C* **102**, 024914 (2020), arXiv:2002.08701 [nucl-ex].
- [13] S. Acharya *et al.* (ALICE), *Phys. Lett. B* **807**, 135564 (2020), arXiv:1910.14396 [nucl-ex].
- [14] M. Stephanov, *Phys. Rev. Lett.* **107**, 052301 (2011), arXiv:1104.1627 [hep-ph].
- [15] J. Adamczewski-Musch *et al.* (HADES), *Phys. Rev. C* **102**, 024914 (2020), arXiv:2002.08701 [nucl-ex].
- [16] M. S. Abdallah *et al.* (STAR), (2021), arXiv:2112.00240 [nucl-ex].

- [17] B. Friman, F. Karsch, K. Redlich, and V. Skokov, *Eur. Phys. J.* **C71**, 1694 (2011), arXiv:1103.3511 [hep-ph].
- [18] W.-j. Fu, X. Luo, J. M. Pawłowski, F. Rennecke, R. Wen, and S. Yin, *Phys. Rev. D* **104**, 094047 (2021), arXiv:2101.06035 [hep-ph].
- [19] A. Bazavov *et al.*, *Phys. Rev. D* **101**, 074502 (2020), arXiv:2001.08530 [hep-lat].
- [20] E. M. Friedlander and R. M. Weiner, *Phys. Rev. Lett.* **43**, 15 (1979).
- [21] N. Fowler, G *et al.*, *Phys. Rev. Lett.* **57**, 3124 (1986).
- [22] S. Gupta, D. Mallick, D. K. Mishra, B. Mohanty, and N. Xu, *Phys. Lett. B* **829**, 137021 (2022).
- [23] K. H. Ackermann *et al.*, *Nucl. Instrum. Meth.* **A499**, 624 (2003).
- [24] B. M. X. Luo, J. Xu and N. Xu, *J. Phys.* **G40**, 105104 (2013), arXiv:1302.2332 [hep-ph].
- [25] M. S. Abdallah *et al.* (STAR), (2021), arXiv:2105.14698 [nucl-ex].
- [26] P. H. M. Cheng *et al.*, *Phys. Rev. D* **70**, 074505 (2009), arXiv:0811.1006 [hep-ph].
- [27] M. Kitazawa and M. Asakawa, *Phys. Rev.* **C86**, 024904 (2012), [Erratum: *Phys. Rev.*C86,069902(2012)], arXiv:1205.3292 [nucl-th].
- [28] A. Bzdak, R. Holzmann, and V. Koch, *Phys. Rev.* **C94**, 064907 (2016), arXiv:1603.09057 [nucl-th].
- [29] A. Bzdak and V. Koch, *Phys. Rev.* **C86**, 044904 (2012), arXiv:1206.4286 [nucl-th].
- [30] T. Nonaka, T. Sugiura, S. Esumi, H. Masui, and X. Luo, *Phys. Rev.* **C94**, 034909 (2016), arXiv:1604.06212 [nucl-th].
- [31] A. Bzdak and V. Koch, *Phys. Rev.* **C91**, 027901 (2015), arXiv:1312.4574 [nucl-th].
- [32] X. Luo, *Phys. Rev.* **C91**, 034907 (2015), arXiv:1410.3914 [physics.data-an].
- [33] X. Luo and T. Nonaka, *Phys. Rev.* **C99**, 044917 (2019), arXiv:1812.10303 [physics.data-an].
- [34] M. Kitazawa, *Phys. Rev.* **C93**, 044911 (2016), arXiv:1602.01234 [nucl-th].
- [35] T. Nonaka, M. Kitazawa, and S. Esumi, *Phys. Rev.* **C95**, 064912 (2017), arXiv:1702.07106 [physics.data-an].
- [36] X. Luo and N. Xu, *Nucl. Sci. Tech.* **28**, 112 (2017), arXiv:1701.02105 [nucl-ex].
- [37] R. Barlow, in *Advanced Statistical Techniques in Particle Physics. Proceedings, Conference, Durham, UK, March 18-22, 2002* (2002) pp. 134–144, arXiv:hep-ex/0207026 [hep-ex].
- [38] T. Sjöstrand, S. Ask, J. R. Christiansen, R. Corke, N. Desai, P. Ilten, S. Mrenna, S. Prestel, C. O. Rasmussen, and P. Z. Skands, *Comput. Phys. Commun.* **191**, 159 (2015), arXiv:1410.3012 [hep-ph].
- [39] B. E. Aboona. *et al.* (STAR), *Phys. Rev. Lett.* **130**, 082301 (2023), arXiv:2207.09837 [nucl-ex].
- [40] F. Gross *et al.*, (2022), arXiv:2212.11107 [hep-ph].
- [41] J. Adam *et al.* (ALICE), *Nature Phys.* **13**, 535 (2017), arXiv:1606.07424 [nucl-ex].
- [42] B. Abelev *et al.* (ALICE), *Phys. Lett. B* **712**, 165 (2012), arXiv:1202.2816 [hep-ex].
- [43] ALICE Collaboration (ALICE), (2022), arXiv:2211.04384 [nucl-ex].
- [44] A. M. Sirunyan *et al.* (CMS), *Phys. Lett. B* **813**, 136036 (2021), arXiv:2009.07065 [hep-ex].
- [45] G. Aad *et al.* (ATLAS), *Phys. Rev. Lett.* **116**, 172301 (2016), arXiv:1509.04776 [hep-ex].
- [46] M. Sakaida, M. Asakawa, H. Fujii, and M. Kitazawa, *Phys. Rev.* **C95**, 064905 (2017), arXiv:1703.08008 [nucl-th].
- [47] M. Abdallah *et al.* (STAR), *Phys. Rev. Lett.* **127**, 262301 (2021), arXiv:2105.14698 [nucl-ex].
- [48] A. Bazavov, D. Bollweg, H. T. Ding, *et al.*, *Phys. Rev. D* **101**, 074502 (2020).